Pseudo-Derivative-Feedback Current Control for Three-Phase Grid-Connected Inverters With *LCL* Filters

Jianguo Wang, *Student Member, IEEE*, Jiu Dun Yan, *Member, IEEE*, and Lin Jiang, *Member, IEEE*.

***Abstract*—Pseudo-derivative-feedback (PDF) control is, for the first time, applied to the current control of three-phase grid-connected inverters with *LCL* filters, which significantly improves the transient response of the system to a step change in the reference input through the elimination of overshoot and oscillation. Two PDF controllers with different terms in the inner feedback path are developed for an inverter current feedback system and a grid current feedback system, respectively. For the inverter current feedback system, a simple PDF controller with a proportional term is used. The influence of the controller parameters on the transient performance is discussed in detail. Compared with a PI controller, the PDF controller is able to eliminate the transient overshoot and oscillation easily while maintaining a fast response. For the gird current feedback system, a PDF controller with a proportional term and a second-order derivative is developed. The implementation and design of the PDF controller are presented. Active damping is achieved with only the feedback from the grid current, and at the same time the system transient response is improved. Both theoretical analysis and experimental results verify the advantages of the PDF control over PI control methods.**

***Index Terms*—Active damping, *LCL* filter, pseudo-derivative-feedback (PDF), three-phase grid-connected inverter, transient response.**

I. Introduction

GRID-CONNECTED inverters form an important interface between distributed power generation systems (DPGSs) and the power grid. The inverter normally acts as a current source, and its operation and control play a crucial role upon the quality of power injected from the DPGSs into the power grid [1]. Requirements for steady-state and transient response are becoming more and more restrictive [2]-[5]. Specifically, in the case of current reference changes, transient response characteristics such as rise time, settling time, overshoot and proper oscillation damping are required to be satisfactory. For example, the overshoot is often limited by the converter current rating, and it is more stringent to limit the overshoot in high power applications [4]. The un-damped oscillations would deteriorate the power quality and create objectionable flicker [2].

J. Wang, J. D. Yan, and L. Jiang are with the Department of Electrical Engineering and Electronics, University of Liverpool, Liverpool, L69 3GJ, U.K. (e-mail: Jianguo.Wang@liv.ac.uk; yaneee@liv.ac.uk; ljiang@liv.ac.uk).

To mitigate high switching frequency harmonics generated by grid-connected inverters, *LCL* filters are widely utilized between the inverter and power grid [6]. Compared with conventional *L*-filters, *LCL* filters have better attenuating ability and require smaller inductance inductors leading to cost-effective solutions [7]. However, the inherent resonance nature of *LCL* filters will degrade the transient response, especially leading to oscillations and overshoots, and may even cause stability problems [8], [9].

Many control strategies have been applied to control the current of grid-connected inverters [9]-[12]. Traditionally, a PI controller is employed in the synchronous rotating frame (SRF) [4], [13], [14], and a PR or damped PR controller in the stationary frame [15]-[18]. In both frames resonant controllers can be applied to attenuate low order harmonics [3], [18]-[20]. Most of previous papers concerned system stability [5], [10], [17], the robustness against grid impedance variations [8], [19], and/or harmonic rejection [18]-[22]. However, the transient response in these studies contains overshoots and oscillations and has not been considered at the design stage, while only examined at simulation or experiment stages. Several other current control techniques, including hysteresis, deadbeat, and nonlinear controllers, have been reported to achieve an improved transient response [1], [3], [23]-[29]. However, these methods are relatively more complicated than the conventional PI and PR controllers.

The PI controller in the SRF is widely used because the control variables become dc signals [3], [16], [30]-[32], and a number of methods have been proposed with an attempt to improve the transient performance of *LCL*-filtered grid-connected inverters. Different tuning methods such as technical optimum (TO), symmetric optimum (SO), and optimized design (OP) have been proposed but cannot eliminate the transient overshoot and oscillation [4], [9], [10], [23]. A common method to reduce the overshoot is decreasing controller gains, which however leads to degraded bandwidth and disturbance rejection capability [8]. A PI state space current control was presented in [4] to improve the rise time and resonance damping, but overshoot still occurs. In [33], controller parameters were optimized using discrete pole-zero plots to achieve a short settling time only. An internal principle model based tuning method was proposed in [23] to optimize the settling time and overshoot of an *L*-filter system by using a smaller PI gain. However, considering the existence of the *LCL* capacitor, design methods proposed for an *L*-filtered system are not applicable to *LCL*-filtered grid-connected inverters.

Another effective alternative strategy is to introduce an additional damping for the *LCL* resonance. Multi-loop based

active damping methods have been researched widely, in which a basic idea is to use inner-loop variables, such as inverter current [6], [15], filter capacitor current [34]-[36] and voltage [35], [37], [38], to form a damping term. However, they require the feedback of more than one signal, which complicates the controller design. Furthermore, most of the controllers are designed for good performances in stability, disturbance rejection, or robustness against to grid impedance variations, resulting in transient responses with overshoot and/or oscillation [15], [34]-[40]. To obtain an improved transient performance, controller parameters should be redesigned, which however would degrade other performances such as the disturbance rejection capability. A second-order derivative method implemented as a high-pass filter has been used in [12], [41], and [42] to provide active damping for grid current. However, there are also significant overshoots and oscillations in the transient response.

This paper applies the pseudo-derivative-feedback (PDF) control method [46]-[48], as an improved strategy over the PI control in the SRF, to improve the transient response of three-phase grid-connected inverters with *LCL* filters to a step change in the reference input via eliminating overshoot and oscillation. The generalized PDF controller is introduced in Section II. Two PDF controllers are then developed for an inverter current feedback system and a grid current feedback system, respectively.

In Section III, a simple PDF controller with a proportional feedback is designed for the inverter current feedback system, which can utilize the inherent damping characteristics of the *LCL* filter [49], [50]. A complete comparison between the performance of PDF and PI controllers is presented. The main merit of the PDF controller is the removal of the additional zero of the closed-loop transfer function and the resultant impact of the transient response from the zero. Compared with the PI controller which can only reduce the overshoot by decreasing the controller gains, the PDF controller completely eliminates the overshoot and oscillation over a wide range of controller parameters.

In Section IV, a PDF controller with a proportional plus a second-order derivative feedback is developed for the grid current feedback system. The practical implementation of the PDF controller is discussed using the Nyquist stability criterion. The stable condition for the controller parameters is derived. Adequate stability margins are ensured by a controller design procedure. The analysis regarding the high-pass filter and system stability is more explicit than that in [12], [41] and [42]. Compared with common active damping methods which require more than one feedback signal, the PDF controller provides active damping with the grid current feedback only, and simultaneously improves the transient response.

Having designed the PDF controllers, experimental results are then presented in Section V to verify their improved performance compared to conventional PI control methods. Conclusions are finally drawn in Section VI.

II. PDF Control for Three-Phase Grid-Connected Inverters With *LCL* Filters

A. PDF Control

A generalized PDF control system is shown in Fig. 1(a). The

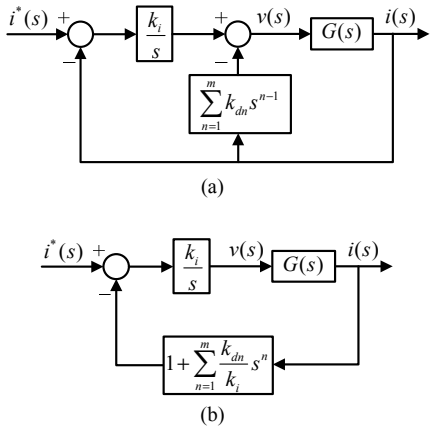

Fig. 1. Generalized PDF control system. (a) System block diagram. (b) Equivalent block diagram.

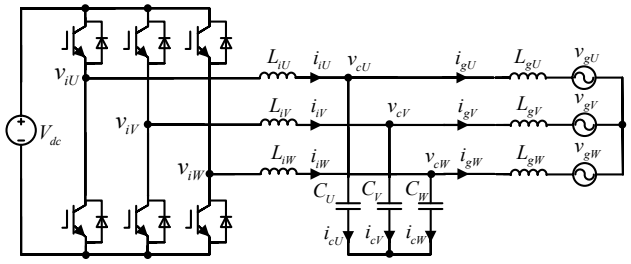

Fig. 2. A three-phase grid-connected inverter with *LCL* filters.

generalized PDF controller comprises two parts: an integral term k_i / s in the forward path, and the superposition of a proportional term k_{d1} and selective derivative terms $k_{dn}s^{n-1}$ (n > 1) in the inner feedback path [46].

The equivalent block diagram is shown in Fig. 1(b) where the second part of the PDF controller is moved to the feedback path which is used to be compared with the reference. It can be seen that the orders of the pseudo-derivative terms are increased by 1, and the proportional term becomes a first-order pseudo-derivative term. This is why the method is called pseudo-derivative-feedback control [46]. The highest order m of the pseudo-derivative terms is not larger than the order of the plant $G(s)$ [46].

B. Three-Phase Grid-Connected Inverter With LCL Filters

The circuit diagram of a three-phase grid-connected inverter with *LCL* filters is shown in Fig. 2, where the inverter is supplied with a constant DC voltage V_{dc}. v_i is the inverter voltage, v_g the grid voltage, and v_c the capacitor voltage. i_i is the inverter current, i_g the grid current, and i_c the capacitor current. The minor parasitic series resistors associated with the inductors are neglected in the modeling, control design, and simulations, in order to represent a worst case in stability and transient response [4], [45], [50]. Parameters of the circuit used in the present work are given in Table I.

By defining voltage and current vectors as:

$$\vec{v_i} = \begin{bmatrix} v_{iU} \\ v_{iV} \\ v_{iW} \end{bmatrix}, \vec{v_c} = \begin{bmatrix} v_{cU} \\ v_{cV} \\ v_{cW} \end{bmatrix}, \vec{v_g} = \begin{bmatrix} v_{gU} \\ v_{gV} \\ v_{gW} \end{bmatrix}, \vec{i_i} = \begin{bmatrix} i_{iU} \\ i_{iV} \\ i_{iW} \end{bmatrix}, \vec{i_g} = \begin{bmatrix} i_{gU} \\ i_{gV} \\ i_{gW} \end{bmatrix}, \quad (1)$$

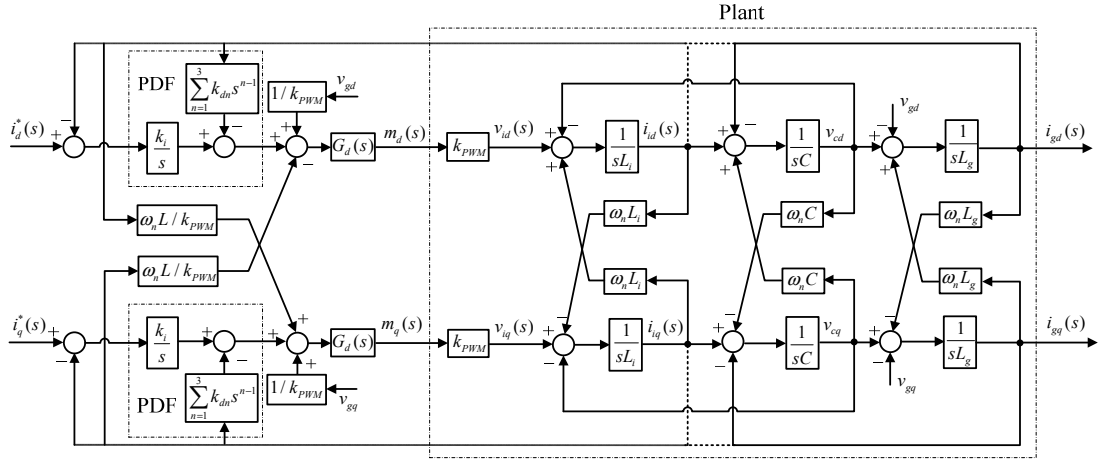

Fig. 3. A three-phase grid-connected inverter with PDF control in the SRF.

TABLE I
PARAMETERS OF THE CIRCUIT

Symbol	Quantity	Value
V_{dc}	DC input voltage amplitude	450 V
V_g	Single-phase grid voltage amplitude	155 V
f_n	Fundamental frequency	50 Hz
L_i	Inverter side inductor	4.4 mH
L_g	Grid side inductor	2.2 mH
C	Capacitor of *LCL* filter	10 μF
f_r	Resonant frequency between L_g and C	1073 Hz
f_{res}	*LCL* resonance frequency	1314.2 Hz
f_s	Sampling and switching frequency	15000 Hz, 6000 Hz

the continuous time dynamic model can be denoted as

$$\begin{cases} L_i \dfrac{d\vec{i_i}}{dt} = \vec{v_i} - \vec{v_c} \\ C \dfrac{d\vec{v_c}}{dt} = \vec{i_i} - \vec{i_g} \\ L_g \dfrac{d\vec{i_g}}{dt} = \vec{v_c} - \vec{v_g} \end{cases} \tag{2}$$

Applying *dq* transformation converts (2) into the following form [19], [52]

$$\begin{cases} L_i \dfrac{d}{dt}\begin{bmatrix} i_{id} \\ i_{iq} \end{bmatrix} + \begin{bmatrix} 0 & -\omega_n L_i \\ \omega_n L_i & 0 \end{bmatrix}\begin{bmatrix} i_{id} \\ i_{iq} \end{bmatrix} = \begin{bmatrix} v_{id} \\ v_{iq} \end{bmatrix} - \begin{bmatrix} v_{cd} \\ v_{cq} \end{bmatrix} \\ C \dfrac{d}{dt}\begin{bmatrix} v_{cd} \\ v_{cq} \end{bmatrix} + \begin{bmatrix} 0 & -\omega_n C \\ \omega_n C & 0 \end{bmatrix}\begin{bmatrix} v_{cd} \\ v_{cq} \end{bmatrix} = \begin{bmatrix} i_{id} \\ i_{iq} \end{bmatrix} - \begin{bmatrix} i_{gd} \\ i_{gq} \end{bmatrix} \\ L_g \dfrac{d}{dt}\begin{bmatrix} i_{gd} \\ i_{gq} \end{bmatrix} + \begin{bmatrix} 0 & -\omega_n L_g \\ \omega_n L_g & 0 \end{bmatrix}\begin{bmatrix} i_{gd} \\ i_{gq} \end{bmatrix} = \begin{bmatrix} v_{cd} \\ v_{cq} \end{bmatrix} - \begin{bmatrix} v_{gd} \\ v_{gq} \end{bmatrix} \end{cases} \tag{3}$$

where $\omega_n = 2\pi f_n$. Subscripts d and q denote corresponding variables in the SRF. v_{id} and v_{iq} are generated from PWM:

$$\begin{cases} v_{id} = m_d k_{PWM} \\ v_{iq} = m_q k_{PWM} \end{cases} \tag{4}$$

where m_d and m_d (m_d, $m_q \in [-1, 1]$) are modulation signals, $k_{PWM} = V_{dc}/2$ is the gain of PWM.

The diagram of the PDF controlled three-phase grid-connected inverter is shown in Fig. 3. Forward decoupling terms $\pm \omega_n L/k_{PWM}$ ($L = L_i + L_g$) are included because the *LCL* filter is similar to an *L*-filter with an inductance of $L_i + L_g$ in the frequency range below the resonance frequency [4], [9], [10], [20]. Since the *LCL*-filtered grid-connected inverter is a third-order system, the highest order m of the pseudo-derivative term is set to 3. The grid voltage feed-forward is used to improve the harmonic attenuation ability [51]. The total delay including computation delay (T_s, $T_s = 1/f_s$) and PWM delay ($0.5T_s$) is described as $G_d(s) = e^{-s1.5T_s}$ [5], [36].

To control the grid current i_g to deliver power to the grid, either the inverter current i_i or grid current i_g can be used as the feedback signal [6]. The transfer functions from v_i to i_i and to i_g are given as (5) and (6), respectively [10], [38], [42], where $\omega_r = 2\pi f_r = \sqrt{1/L_g C}$ and $\omega_{res} = 2\pi f_{res} = \sqrt{(L_i + L_g)/L_i L_g C}$.

$$G_{i_i v_i}(s) = \frac{i_i(s)}{v_i(s)} = \frac{s^2 + \omega_r^2}{sL_i(s^2 + \omega_{res}^2)} \tag{5}$$

$$G_{i_g v_i}(s) = \frac{i_g(s)}{v_i(s)} = \frac{\omega_r^2}{sL_i(s^2 + \omega_{res}^2)} \tag{6}$$

In the following sections, two PDF controllers with different terms in the inner feedback path are developed for the inverter current and grid current feedback systems, respectively.

III. PDF FOR INVERTER CURRENT FEEDBACK SYSTEM

The inverter current can be used as the feedback variable to indirectly control the grid current based on the following two reasons. Firstly, the inverter current is usually used to protect the power circuits in industrial applications [7]. Secondly, it can utilize the inherent damping characteristics of the *LCL* filter to neutralize its resonance to enhance system stability [50]. A single-loop controlled inverter current feedback system can be made stable on condition that f_s is larger than $6f_{res}$ (for the general case with a total time delay of $1.5T_s$) [5], [37], [49]. Using f_s = 15000 Hz, the ratio of f_s to f_{res} is 11.4, which meets the stability condition with adequate margins (a ratio larger than 9 for a phase margin (PM) of 30°) [5].

In this section, a simple PDF controller with the inner feedback path employing only a proportional term is designed for the inverter current feedback system. In terms of structure, the difference between the PDF controller and PI controller

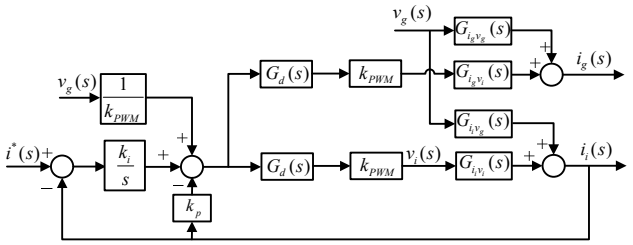

Fig. 4. Block diagram of the PDF controlled inverter current feedback system.

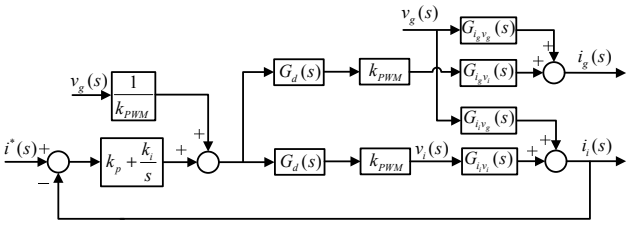

Fig. 5. Block diagram of the PI controlled inverter current feedback system.

rests with the change of the position for the proportional term. However, overshoot and oscillation in the transient response caused by reference changes, which are unavoidable for the PI controller, can be easily eliminated by the PDF controller.

A. Control Loops

1) Continuous s-Domain Loop: The *s*-domain block diagram of an inverter current feedback system controlled by the simple PDF controller is shown in Fig. 4. The transfer functions from v_g to i_i and to i_g are $G_{i_i v_g}(s) = \frac{i_i(s)}{v_g(s)} = \frac{-\omega_r^2}{sL_i(s^2+\omega_{res}^2)}$ and $G_{i_g v_g}(s) = \frac{i_g(s)}{v_g(s)} = -\frac{s^2 L_i C + 1}{sL_i L_g C(s^2+\omega_{res}^2)}$, respectively. The block diagram of a PI controlled inverter current feedback system is shown in Fig. 5. It can be seen that the difference between the PDF and PI controllers is the change of the position of k_p.

The closed-loop transfer function of the PDF control system is given as

$$G_{clPDF}(s) = \frac{i_g(s)}{i^*(s)} = \frac{k_i G_d(s) k_{PWM} G_{i_g v_i}(s)}{(k_p s + k_i) G_d(s) k_{PWM} G_{i_i v_i}(s) + s}, \quad (7)$$

while that of the PI control system is expressed as

$$G_{clPI}(s) = \frac{i_g(s)}{i^*(s)} = \frac{(k_p s + k_i) G_d(s) k_{PWM} G_{i_g v_i}(s)}{(k_p s + k_i) G_d(s) k_{PWM} G_{i_i v_i}(s) + s}. \quad (8)$$

As seen the PI system has one more closed-loop zero ($s = -K = -k_i / k_p$) than that of the PDF system. However their loop gains are identical provided that identical controller parameters are used, thus the same stability characteristics.

It can be derived from Fig. 4 and Fig. 5 that the PDF and PI systems have an identical closed-loop transfer function from the grid voltage to grid current, given as

$$G_{gd}(s) = \frac{i_g(s)}{v_g(s)} = \frac{\left[s - (sk_p + k_i) k_{PWM} G_{i_i v_g}(s) \right] G_d(s) G_{i_g v_i}(s)}{(k_p s + k_i) G_d(s) k_{PWM} G_{i_i v_i}(s) + s} + G_{i_g v_g}(s), \quad (9)$$

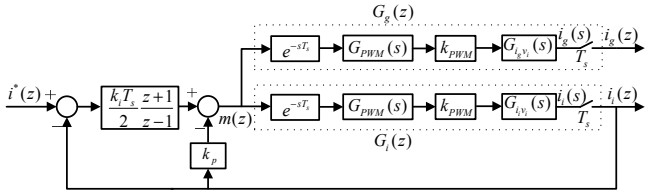

Fig. 6. Block diagram of digitally controlled inverter current feedback system with the PDF controller.

which implies that their disturbance rejection ability for grid voltage harmonics are identical when the same parameters are used.

2) Discrete z-domain Loop: The block diagram of digitally controlled grid-connected inverter with the PDF controller is shown in Fig. 6. v_g is omitted because it is considered as disturbance [42], [50]. The integral term is discretized using the Tustin's method. The computation delay is described as e^{-sT_s}. The PWM is modeled as a zero-order-hold (ZOH): $G_{PWM}(s) = (1 - e^{-sT_s}) / s$ [19], [36]. To obtain the discrete closed-loop transfer function, the transfer function from $m(z)$ to $i_i(z)$ and $i_g(z)$ should be obtained first. Therefore *z*-transform is used to obtain the discrete transfer functions of the paths which contain the processing delay, PWM, and the plant transfer functions $G_{i_i v_i}(s)$ and $G_{i_g v_i}(s)$ followed by ideal samplers [6]. The transfer functions from $m(z)$ to $i_i(z)$ and $i_g(z)$ are derived as (10) and (11), respectively [5].

$$G_i(z) = Z\{e^{-sT_s} G_{PWM}(s) k_{PWM} G_{i_i v_i}(s)\} = \frac{k_{PWM}}{(L_i + L_g) z} \left(\frac{T_s}{z-1} + \frac{L_g \sin \omega_{res} T_s}{L_i \omega_{res}} \frac{z-1}{z^2 - 2z\cos\omega_{res} T_s + 1} \right) \quad (10)$$

$$G_g(z) = Z\{e^{-sT_s} G_{PWM}(s) k_{PWM} G_{i_g v_i}(s)\} = \frac{k_{PWM}}{(L_i + L_g) z} \left(\frac{T_s}{z-1} - \frac{\sin \omega_{res} T_s}{\omega_{res}} \frac{z-1}{z^2 - 2z\cos\omega_{res} T_s + 1} \right) \quad (11)$$

The discrete closed-loop transfer functions of the PDF and PI systems are expressed as

$$G_{clPDF}(z) = \frac{i_g(z)}{i^*(z)} = \frac{k_i T_s (z+1) G_g(z)}{2z - 2 + \left[(2k_p + k_i T_s) z - 2k_p + k_i T_s \right] G_i(z)} \quad (12)$$

and

$$G_{clPI}(z) = \frac{i_g(z)}{i^*(z)} = \frac{\left[(2k_p + k_i T_s) z - 2k_p + k_i T_s \right] G_g(z)}{2z - 2 + \left[(2k_p + k_i T_s) z - 2k_p + k_i T_s \right] G_i(z)} \quad (13)$$

respectively. As seen from (12) and (13) in the *z*-domain the difference between the PDF and PI systems is the modification of one closed-loop zero ($z = -1$ for PDF and $(2k_p - k_i T_s) / (2k_p + k_i T_s)$ for PI).

B. Transient Responses

The same as the PI control system, the stability of the PDF system is mainly determined by the proportional gain k_p [8], [34], hence the stability boundary of k_p is investigated first. The

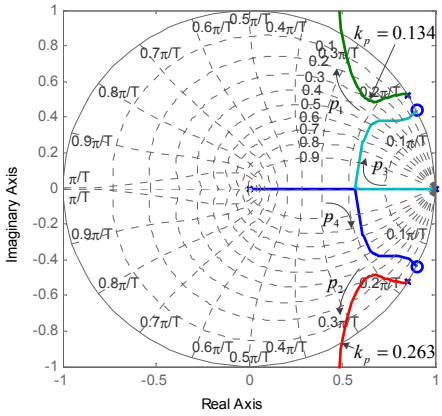

Fig. 7. Root loci of the inverter current feedback system controlled by a proportional compensator.

root loci based on a proportional compensator are shown in Fig. 7, where the arrows indicate the changing directions of four poles (p_1-p_4) when k_p increases. p_1 and p_2 are caused by the *LCL* resonance and are generally the dominant poles, p_3 is due to the inductors and p_4 due to the time delay [4]. The stable boundary of k_p is 0.263. To guarantee a gain margin (GM) of 3 dB, k_p should be set to a value smaller than 0.186. When $k_p = 0.134$, the system would have the fastest step response, as the dominant poles p_1 and p_2 are farthest away from the unit circle boundary.

Because the grid current i_g is indirectly controlled by the inverter current i_i, i_q^* is set to $\omega_n C V_g$ instead of zero to achieve unity power factor [50]. With a unit step change in i_d^*, the simulated step responses of the PDF system with $k_p = 0.134$ and different values of K are shown in Fig. 8(a), while those of the PI system are shown in Fig. 8(b) (the simulation was performed in the discrete system of Fig. 3; the simulated *d*-axis current responses are almost identical to the step responses of the closed-loop transfer functions (12) and (13)). As can be seen, in the PI control systems obvious couplings exist because of the time delay and un-decoupled capacitor, whereas the coupling in PDF systems is much milder and even negligible. Concerning the response in the *d*-axis current, it is obvious that there are overshoots (60% - 100%) and oscillations in the PI system, and the overshoot increases when K rises. By contrast, much smoother responses are obtained by the PDF controller, in spite that mild overshoot also appears when a large K is used. Although the rise time of the PDF system is longer than that of the PI system, its settling time is relatively shorter than that of the latter when K is large ($K = 1400$: $t_{sPDF} = 2.24$ ms, $t_{sPI} = 2.51$ ms; $K = 2000$: $t_{sPDF} = 1.83$ ms, $t_{sPI} = 2.75$ ms. A tolerance band of 1% is defined for the settling time [23]). The slower response of the PDF system with a small K will be discussed later in Section III-C. It can be seen that $k_p = 0.134$ and $K = 1400$ are the suitable parameters for the PDF controller to give a satisfactory transient response, with a fast response and no overshoot or oscillation.

There are many parameter optimization methods for the PI controller to optimize its performance, such as the SO [9], [35] and OP [53]. Parameters of SO and OP are tuned to have the values

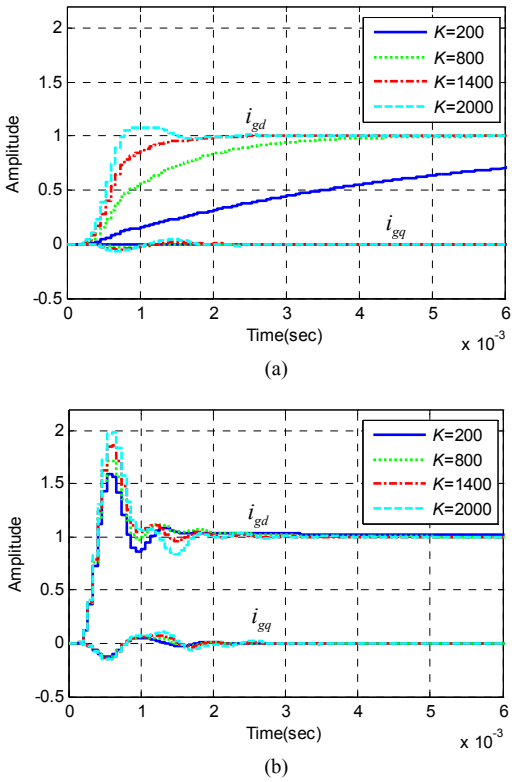

Fig. 8. Step responses for $k_p = 0.134$ with different values of K (k_i/k_p). (a) PDF control system. (b) PI control system.

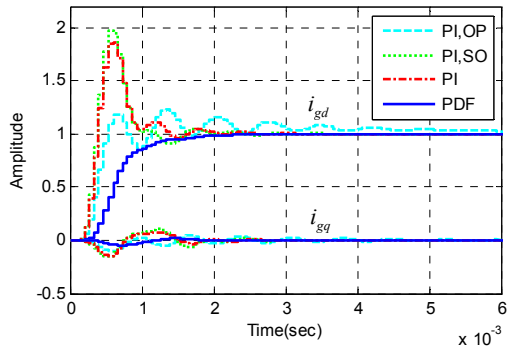

Fig. 9. Step responses of the PDF control system and PI system with different design methods.

$$k_p = \frac{L_i + L_g}{3k_{PWM}T_s}, K = \frac{1}{9T_s} \tag{14}$$

and

$$k_p = \frac{\omega_c(L_i + L_g)}{k_{PWM}}, K = \frac{\omega_c}{10} \tag{15}$$

respectively, ω_c in (15) is the crossover frequency that can be chosen as $\omega_c = 0.3\omega_{res}$ [50]. The step responses of the PI system with the optimized parameters (14) and (15), and those of the PI and PDF systems with $k_p = 0.134$ and $K = 1400$ are shown in Fig. 9. It can be seen that the PI controller always gives overshoot and oscillation. Particularly the settling time of the PI system with OP is much longer than that of the PDF system. The advantage of the PDF controller over PI controller in the transient response is obvious.

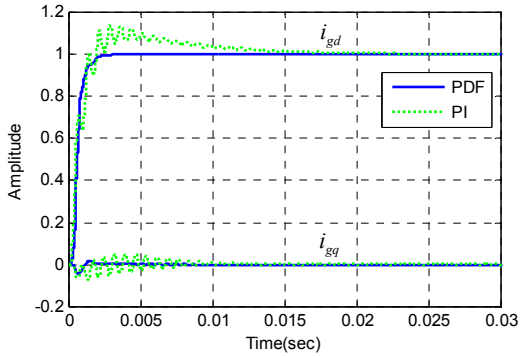

Fig. 10. Step responses of PDF and PI control systems with the same rise time.

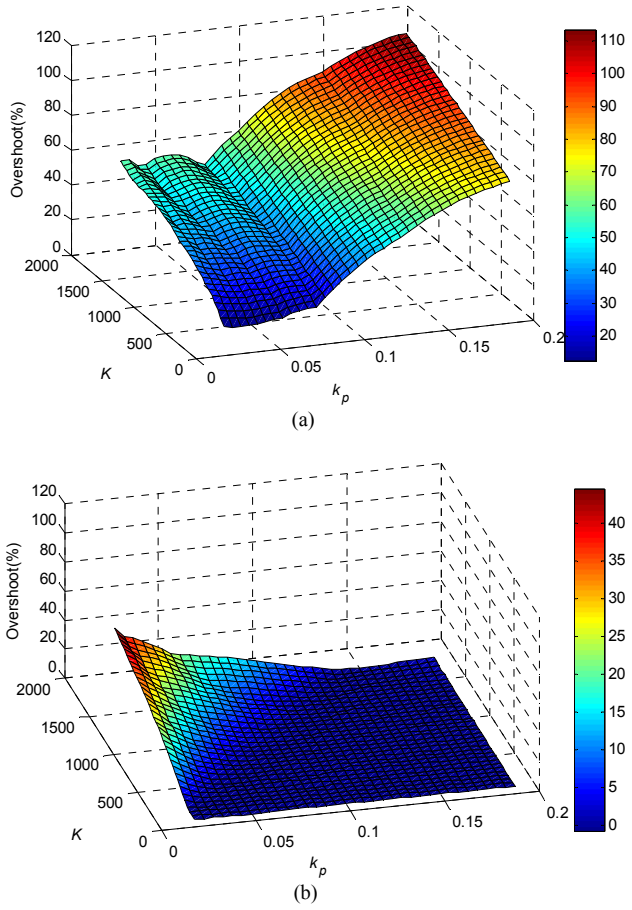

Fig. 11. Overshoots of PI and PDF control systems with different controller parameters. (a) PI controller. (b) PDF controller.

When the PI controller is tuned to give an identical rise time as the PDF controller (0.96 ms, from 10% to 90%), the step responses are presented in Fig. 10, which shows that the PI controller (k_p = 0.035, K = 150) still produces overshoot and oscillation. Furthermore, the settling time of the PI system (15 ms) is about 7 times that of the PDF system (2.24 ms).

In fact, there are unavoidable overshoots in the PI system, whereas the PDF controller can achieve an over-damping transient easily. Overshoots of the PI system and PDF system with varied k_p and K values are shown in Fig. 11(a) and (b) respectively. As seen, the overshoot generated by the PI

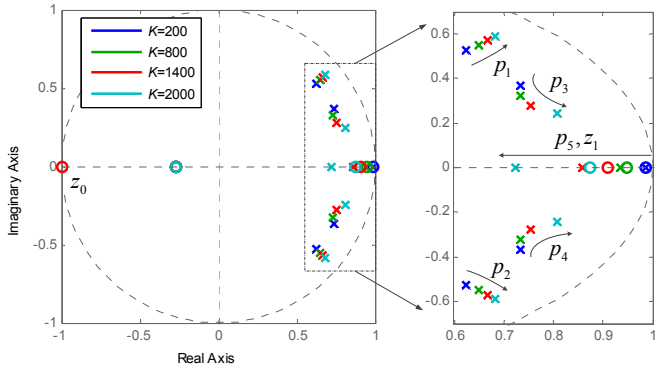

Fig. 12. Pole-zero map of the PI and PDF systems with k_p = 0.134 and different values of K.

controller ranges from 20% to 110%. To reduce the overshoot, smaller controller gains have to be used, resulting in a lower bandwidth and disturbance rejection ability [23], [38]. In contrast, no overshoot exists in the PDF system over a wide range of controller parameters. Although overshoot appears when the PDF controller employs a small k_p and large K, it is much smaller than that of the PI system. Therefore the PDF controller can achieve a better transient performance without degrading the bandwidth and disturbance rejection ability.

C. Discussion of Influence of Controller Parameters on the Transient Response

Corresponding to the transient responses of the PDF and PI systems in Fig. 8, the closed-loop pole-zero map is shown in Fig. 12 (a zero outside the unit circle is omitted for a better view), where the arrows indicate the changing directions of poles and zeroes as K increases. In comparison with Fig. 7, the additional pole p_5, zeroes z_0 and z_1 are introduced by the controllers. The difference between the PDF and PI systems, as demonstrated in (12) and (13), is that the zero $z_0 = -1$ is affiliated only to the PDF system whereas $z_1 = (2k_p - k_iT_s) / (2k_p + k_iT_s)$ is only to the PI system. With a small K value of 200, for the PI system p_5 and z_1 are canceled by each other, but for the PDF system p_5 is the dominant pole which is near the unit circle, leading to a slow transient response (see Fig. 8(a)). When K increases, the dynamics of the PDF system becomes faster since p_5 moves more inside of the unit circle. Meanwhile, for the PI system p_5 is not canceled by z_1, the PI and PDF systems have identical closed-loop poles. Hence the times for the two systems to reach their steady-state values are approximately identical. When K is sufficiently large (= 2000), p_1 and p_2 are less damped, leading to mild overshoot and oscillation in the PDF system.

IV. PDF FOR GRID CURRENT FEEDBACK SYSTEM

A single-loop PI controller can stabilize a grid current feedback system if $2f_{res} < f_s < 6f_{res}$ [5], [45], [49], and in this case a simple PDF controller can be adopted to improve the transient response. However, this region is not attractive because the grid impedance variation in weak grids may shift f_{res} in a wide spectrum across the point of f_s / 6, which would trigger instability [5], [8], [19]. Instead, an additional inner

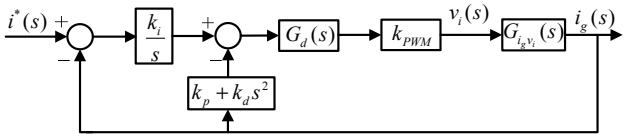

Fig. 13. Block diagram of the PDF controlled grid current feedback system.

active damping feedback loop is needed, but more than one signal is to be sensed [34]-[40]. A second-order derivative method implemented as a high-pass filter has been used in [12], [41], and [42] to provide active damping for the grid current. However, the time delay is not considered in [41], thus the analysis of the control loop can potentially be unreliable [43]-[45]. In [42], the design of the outer current controller is conducted before that of the inner loop, which would lead to inadequate stability margins or even an unstable system. In [12], the critical value for the cutoff frequency to ensure a positive virtual resistance has been discussed, but the relationship between the filter's cutoff frequency and gain to guarantee a stable inner active damping loop was not studied. Moreover, the co-design flow for control parameters and the stability analysis of the overall system are vague. In all cases, it is difficult for the PI plus active damping methods to eliminate the transient overshoot and oscillation [34]-[42].

In this section, a PDF controller with a proportional gain and a second-order derivative in the inner feedback path is developed for the grid current feedback system. Active damping is achieved with the grid current feedback only. In addition to giving a stable operation, the PDF controller can also respond without overshoot to a step change in the reference input. A controller design procedure is proposed to ensure adequate stability margins and satisfactory transient performances, and it is superior to the tuning methods in [12], [41], and [42].

A. Control Loops

The block diagram of the PDF controlled grid current feedback system is shown in Fig. 13. In comparison to the simple PDF controller for the inverter current feedback system, a second-order derivative term $k_d s^2$ is included in the inner feedback path.

For the sake of simplicity in stability analysis, the feedback loop with the second-order derivative is treated as an inner loop. The Nyquist stability criterion is used to explain why the inner loop can be stabilized, i.e., active damping is achieved. In the open-loop Bode diagram, only the frequency ranges with magnitudes above 0 dB are concerned. For the phase plot in these ranges, a $\pm (2k + 1)\pi$ crossing in the direction of phase rising is defined as positive crossing, while a crossing in the direction of phase falling is defined as negative crossing [36]. The numbers of the positive and negative crossings are denoted as N_+ and N_- respectively. According to the Nyquist stability criterion, the number of the open-loop unstable poles P must equal $2(N_+ - N_-)$ to ensure system stability, i.e., $P = 2(N_+ - N_-)$ [5], [36]. It is obvious that $P = 0$, hence $N_+ - N_- = 0$ is required.

The Bode diagrams of the inner loop gain with and without $k_d s^2$, i.e., $T_i(s) = G_d(s) k_{PWM} G_{i_g v_i}(s) k_d s^2$ and $G_d(s) k_{PWM} G_{i_g v_i}(s)$, are shown in Fig. 14. It is obvious that $N_+ = 0$, thus $N_- = 0$ is

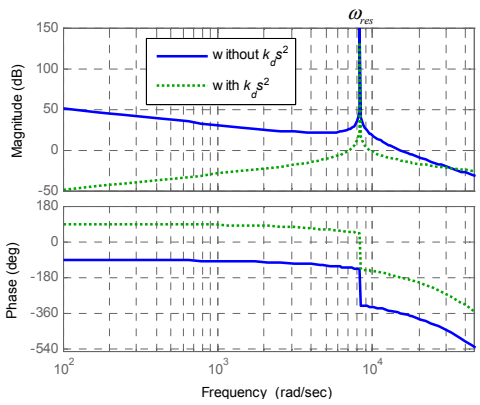

Fig. 14. Bode diagrams of the inner loop gain $T_i(s)$, with and without $k_d s^2$.

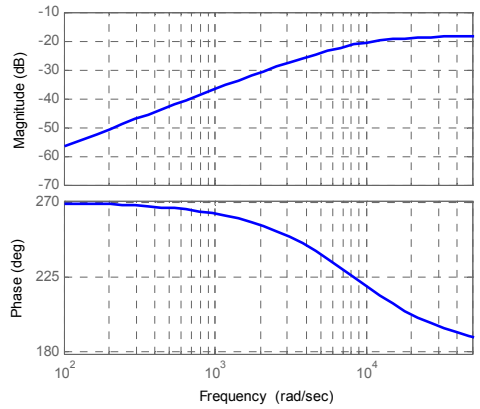

Fig. 15. Bode diagram of the high-pass filter with a negative gain

required for stability. Without $k_d s^2$, there is a negative crossing at ω_{res} (the phase crosses over –180° while the magnitude is positive infinite because of the resonance pole [5]), whereas with $k_d s^2$ the phase is increased by 180° such that it may not cross over –180° at ω_{res}. Therefore, if k_d is tuned to make the magnitude gains below 0 dB at frequencies where the phase crosses 180° or –180°, no negative crossing will exist and the inner loop is stabilized.

B. Implementation of the Second-Order Derivative

However, the second-order derivative will dramatically amplify noise disturbances, which would lead to unreasonable consequences [41], [42]. Therefore, the practical implementation of $k_d s^2$ should be developed.

From the previous analysis, it can be summarized that to achieve the damping effect of the second-order derivative $k_d s^2$, a phase lead of 180° or over at ω_{res} and magnitude attenuation in low frequency range are required for the alternative method. A high-pass filter with a negative gain can achieve this target and avoid the influence of noises [12], [41], [42]:

$$G_{hp}(s) = -\frac{s k_{hp}}{s + \omega_{hp}}, \tag{16}$$

where ω_{hp} is the cut-off angular frequency (should be in the range of $(0, 0.5\omega_s]$ [12], $\omega_s = 2\pi f_s$). The Bode diagram of (16) shown in Fig. 15 illustrates a phase lead between 180° and 270° and high attenuation in low frequency range.

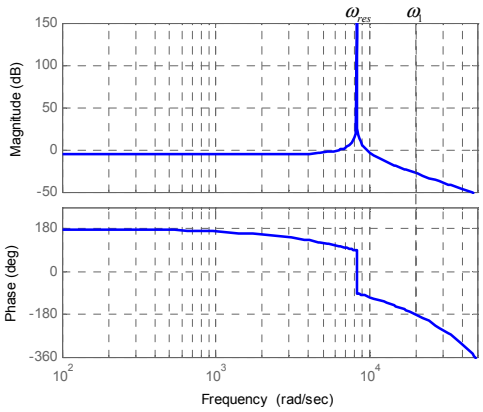

Fig. 16. Bode diagram of the high-pass filter active damping loop gain.

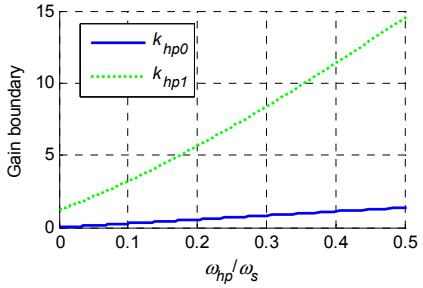

Fig. 17. Gain boundaries k_{hp0} and k_{hp1} as a function of ω_{hp}/ω_s for the case with f_s = 15000 Hz.

C. Tuning of Controller Parameters

1) Inner Active Damping Loop: The Bode diagram of the inner loop gain $T_i(s) = G_d(s)k_{PWM}G_{i_g v_i}(s)G_{hp}(s)$ is shown in Fig. 16. The magnitude (in decibels) and phase of $T_i(s)$ are given as (17), shown at the bottom of this page.

As can be seen, the phase starts from 180° at ω = 0, and crosses over –180° at a frequency ω_1. The frequency ω_1, which should be larger than ω_{res} to avoid the negative crossing at ω_{res} (i.e., the phase does not cross over –180° at ω_{res}), can be obtained by solving the following equation:

$$\frac{3\pi\omega_1}{\omega_s} + \arctan\frac{\omega_1}{\omega_{hp}} = \pi. \tag{18}$$

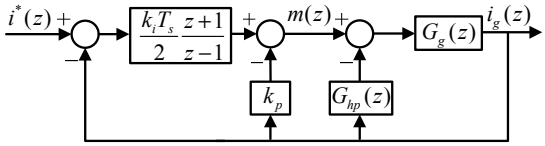

Fig. 18. Discrete block diagram of the PDF controlled grid current feedback system.

It is interesting to note that ω_1 from (18) is identical to the 'critical frequency' in [12] below which a positive virtual resistance is achieved. The requirement for ω_{hp} can also be deduced to ensure $\omega_1 > \omega_{res}$ (i.e., a positive virtual resistance at ω_{res} [12]), whereby the inner loop is possible to be stable [12]. However, the possible stability is not enough, the stable condition for k_{hp} should be also derived. As explained above, if the magnitudes in (17) are tuned to be below 0 dB at ω = 0 (the phase crosses 180°) and ω_1 (the phase crosses –180°), no negative crossing exists, and the inner loop is stabilized. Therefore, with a given ω_s and a proper ω_{hp}, the two gain boundaries for k_{hp} are deduced as (19), and the smaller one of k_{hp0} and k_{hp1} is the critical value.

$$\begin{cases} k_{hp0} = \dfrac{(L_i + L_g)\omega_{hp}}{k_{PWM}} \\ k_{hp1} = \dfrac{L_i(\omega_1^2 - \omega_{res}^2)\sqrt{\omega_1^2 + \omega_{hp}^2}}{k_{PWM}\omega_r^2}. \end{cases} \tag{19}$$

With a high f_s = 15000 Hz = 11.4ω_{res}, it is indicated in (18) and also [12] that a positive ω_{hp} is adequate for the possible stability. In this case, the curves of the gain boundaries in (19) as a function of ω_{hp}/ω_s are shown in Fig. 17. It can be seen that k_{hp0} is always smaller than k_{hp1}, hence k_{hp} can be chosen as $k_{hp} = k_{hp0}/2 = (L_i + L_g)\omega_{hp}/2k_{PWM}$. ω_{hp} is to be tuned later to obtain adequate stability margins for the whole loop.

The z-domain block diagram of the grid-connected inverter with the PDF controller is shown in Fig. 18, where $G_{hp}(z)$ is the Tustin's discrete equivalent of $G_{hp}(s)$, given by

$$G_{hp}(z) = -\frac{2k_{hp}(z-1)}{(\omega_{hp}T_s + 2)z + \omega_{hp}T_s - 2}. \tag{20}$$

The discrete inner loop gain $T_i(z) = G_g(z)G_{hp}(z)$ is given as (21), shown at the bottom of this page. The closed-loop transfer function of the inner loop is expressed as

$$\begin{cases} 20\lg\left|T_i(s)\right|_{s=j\omega}\right| = 20\lg\left|e^{-j\omega 1.5T_s}k_{PWM}\dfrac{\omega_r^2}{L_i(\omega_{res}^2 - \omega^2)}\dfrac{-k_{hp}}{j\omega + \omega_{hp}}\right| = 20\lg\left(\dfrac{k_{PWM}\omega_r^2}{L_i\left|\omega_{res}^2 - \omega^2\right|}\dfrac{k_{hp}}{\sqrt{\omega^2 + \omega_{hp}^2}}\right), \\ \angle T_i(s)\big|_{s=j\omega} = \angle e^{-j\omega 1.5T_s}k_{PWM}\dfrac{\omega_r^2}{L_i(\omega_{res}^2 - \omega^2)}\dfrac{-k_{hp}}{j\omega + \omega_{hp}} = \begin{cases} -\dfrac{3\omega T_s}{2} + \pi - \arctan\dfrac{\omega}{\omega_{hp}}, \omega < \omega_{res} \\ -\dfrac{3\omega T_s}{2} - \arctan\dfrac{\omega}{\omega_{hp}}, \omega > \omega_{res}. \end{cases} \end{cases} \tag{17}$$

$$T_i(z) = -\frac{2k_{PWM}k_{hp}}{(L_i + L_g)\omega_{res}}\frac{z^2(\omega_{res}T_s - \sin\omega_{res}T_s) + z(2\sin\omega_{res}T_s - 2\omega_{res}T_s\cos\omega_{res}T_s) + \omega_{res}T_s - \sin\omega_{res}T_s}{[(\omega_{hp}T_s + 2)z + \omega_{hp}T_s - 2](z^3 - z^3 2\cos\omega_{res}T_s + z)} \tag{21}$$

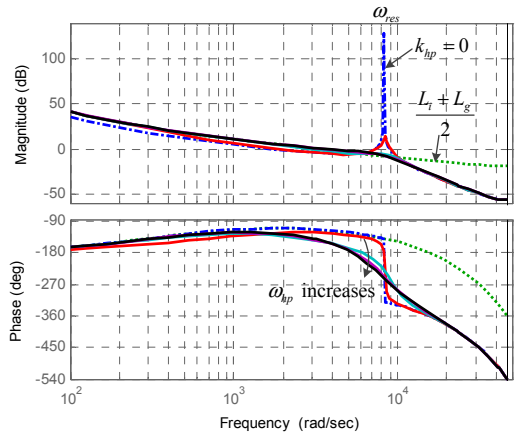

Fig. 19. Bode diagrams of the loop gain $T(z)$ with varied ω_{hp}.

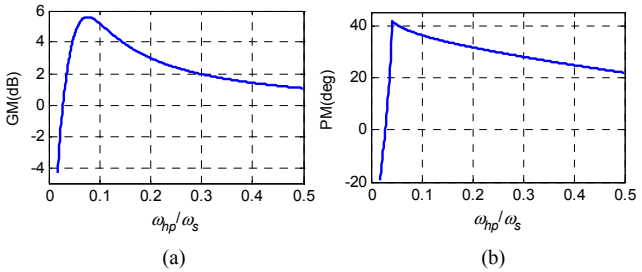

(a) (b)

Fig. 20. Relationship between stability margins and ω_{hp}/ω_s. (a) Gain margin (GM). (b) Phase margin (PM).

$$G_{cli}(z)=\frac{i_g(z)}{m(z)}=\frac{G_g(z)}{1+T_i(z)}. \tag{22}$$

In the frequency range below ω_{res}, $G_g(z)$ is similar to an L-filter with an inductance of $L_i + L_g$ [39], [45], [50]. The discrete transfer function of the L-filter is given as

$$G_L(z)=Z\left\{\frac{e^{-sT_s}G_{PWM}(s)k_{PWM}}{s(L_i+L_g)}\right\}=\frac{k_{PWM}T_s}{(L_i+L_g)z^2-(L_i+L_g)z} \tag{23}$$

With $k_{hp}=(L_i+L_g)\omega_{hp}/2k_{PWM}$, $T_i(z)\approx -1/2$, hence $G_{cli}(z)=2G_g(z)\approx 2G_L(z)$. It means that the inner loop approximately behaves as an L-filter with an inductance of $(L_i+L_g)/2$ in the frequency range below ω_{res}.

2) Outer Loop: Since the loop from $m(z)$ to $i_g(z)$ has been treated as an inner loop, there is an outer loop with a simple PDF controller that was used in the inverter current feedback system. As discussed in Section III, the loop gain of the outer loop with a simple PDF controller is identical to that with a PI controller. Therefore the loop gain is $T(z)=G_{PI}(z)G_{cli}(z)$, where $G_{PI}(z)=k_p+k_iT_s(z+1)/2(z-1)$ is the discrete transfer function of the PI controller.

Because $G_{cli}(z)$ is similar to an L-filter with an inductance of $(L_i+L_g)/2$ below ω_{res}, the simple outer PDF controller can be designed based on the method in (15). [45] and [50] suggested that ω_c equal to or be larger than $0.3\omega_{res}$, in the present work $\omega_c = 0.4\omega_{res}$ is used to obtain adequate stability margins and a larger bandwidth so that a better transient response is achieved. As a result k_p and k_i are tuned to

$$k_p=\frac{\omega_{res}(L_i+L_g)}{5k_{PWM}}, k_i=\frac{k_p\omega_{res}}{25}. \tag{24}$$

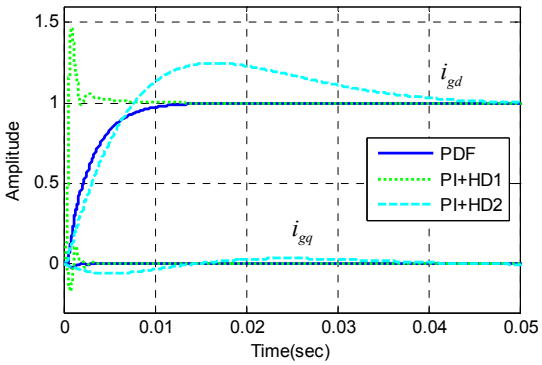

Fig. 21. Step responses of the PDF system and PI plus high-pass filter active damping control system, with f_s = 15000 Hz.

With the designed k_{hp}, k_p, and k_i, the Bode diagrams of $T(z)$ with varied values of ω_{hp} are shown in Fig. 19. The case with $\omega_{hp}=0$ (i.e., $k_{hp}=0$) is the one without the inner active damping term. The open-loop Bode diagram of an L-filter system with an inductance of $(L_i + L_g) / 2$ controlled by the simple PDF controller is also plotted, it reveals that $G_{cli}(z)$ is similar to this L-filter below ω_{res}. As seen from Fig. 19, a small ω_{hp} cannot effectively damp the LCL resonance, and the system is even unstable. On the other hand, with a large ω_{hp} the phase lag is increased, leading to small stability margins. To pick a satisfactory ω_{hp}, the relationship between stability margins and ω_{hp}/ω_s is illustrated in Fig. 20. It can be seen that $\omega_{hp}=\omega_{res}$ ($\omega_{hp}/\omega_s=0.0876$) is a good option, with which GM = 5.5 dB and PM = 37.4°.

As the grid current i_g is controlled directly, i_q^* is set to 0. With a unit step change in i_d^*, the step response of the PDF controlled grid current feedback system is shown in Fig. 21. Apparently, a smooth transient without overshoot is produced. For comparison, the system controlled by a PI plus high-pass filter active damping method [12], [41], [42], is also tested in two scenarios, one with the same parameters (k_p = 0.0484, k_i = 15.972) as those of the PDF controller, and the other with the same rise time (5.97 ms) as the latter by reducing the PI gains ($k_p=0.003$, $k_i=0.24$). Identical high-pass filter parameters are used in the PDF and PI systems. In the first scenario, the transient contains oscillation and great overshoot (47%), while in the latter scenario, an overshoot of 25% exists and the settling time is over three times that of the PDF system (41.8 ms versus 12.8 ms). Moreover, the coupling between d- and q-axis currents in the PDF system is much milder than that in the PI systems. Similar to the simple PDF controller used for the inverter current feedback system, the PDF controller for the grid current feedback system can achieve a well-damped transient response over a wide range of control gains, whereas the PI method can only reduce the overshoot by using small gains.

D. Performance at Low Sampling Frequency

It is known that the time delay may impose influence on the transient response [12], [43]-[45]. To evaluate the influence on the PDF controller, the system with a lower sampling frequency f_s = 6000 Hz ($f_s/f_{res}=4.567$, $f_{res}/f_s=0.219$) is examined. It can be deduced from (18) that ω_{hp} should be larger than $0.1177\omega_s$ to

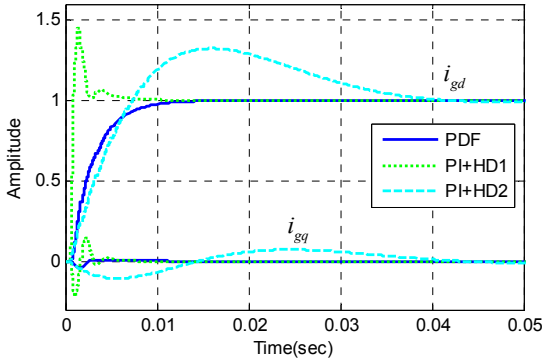

Fig. 22. Step responses of the PDF system and PI plus high-pass filter active damping control system, with f_s = 6000 Hz.

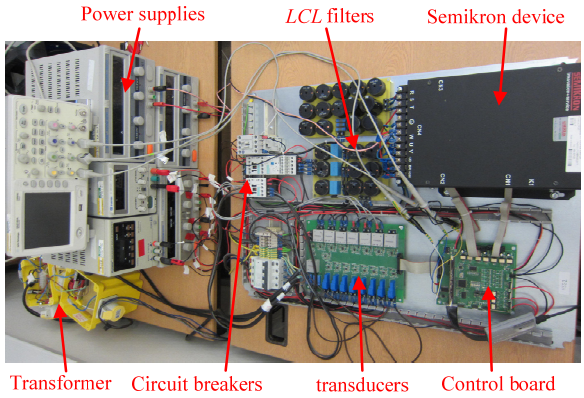

Fig. 23. The three-phase *LCL*-filtered grid-connected inverter prototype used in experiments.

ensure $\omega_1 > \omega_{res}$. Therefore, $\omega_{hp} = 0.5\omega_s$ can be chosen to achieve a robust damping [12]. Then ω_1 is obtained as $0.279\omega_s$ from (18). In this case $k_{hp0} = 0.5489$ and $k_{hp1} = 0.392$ are calculated from (19). As seen k_{hp1} is smaller than k_{hp0}, contrary to the case with f_s = 15000 Hz. Hence k_{hp} can be set to $k_{hp1} / 2$. k_p and k_i are still tuned according to (24). With the designed PDF controller, GM = 5.86 dB and PM = 37.7°.

Similar to Fig. 21, the step responses of the PDF and PI plus high-pass filter active damping control systems are shown in Fig. 22. As expected, the transient response of the PDF system is smooth without overshoot. The PI controlled systems, in contrast, exhibit large overshoot (45% and 31%) or a longer settling time (38.1 ms versus 12.2 ms of the PDF system; k_p = 0.0045 and k_i = 0.45). These results further verify the advantage of the PDF controller even at a low sampling frequency.

V. Experimental Results

To verify the better performance of the two PDF controllers compared to conventional controllers, experimental tests were implemented in a DSP controlled three-phase grid-connected inverter prototype, as shown in Fig. 23. The prototype comprises a Semikron power processing device (contains a three-phase IGBT inverter), a main DSP control board (TMS320F28335), a three-phase *LCL* circuit, several circuit breakers, voltage/current transducers with I/O conditioning circuits, and an isolated step-up transformer (primary voltage: 230 V_{RMS} (line to neutral), second voltage: 110 V_{RMS} (line to neutral)). Parameters of the circuit are given in Table I, and the controller parameters obtained previously are used for corresponding experiments.

A. PDF for Inverter Current Feedback System

Firstly, the steady-state response of the PDF control system with $i_d^* = 4$ A was performed. Fig. 24 shows the steady-state one-phase grid voltage (THD ≈ 1.9%) and current (THD ≈ 2.7%). It illustrates that the grid current is in phase with grid voltage. Note that a same current quality would be obtained by the PI system when identical controller parameters are used because of the identical disturbance rejection ability.

The transient responses with i_d^* stepping from 1 A to 4 A have been tested. With the parameters obtained before (k_p = 0.134, K = 1400), the output currents of the PDF and PI systems are shown in Fig. 25 and Fig. 26, respectively. The settling time of the PI system is about 4 ms, longer than that of the PDF system (2.5 ms). Moreover, the PI system contains great overshoots (53% in i_{id} and 67% in i_{gd}, slightly different from simulation results because of issues such as the minor parasitic resistors and the variation of circuit parameters) and oscillations, whereas the transient response of the PDF system is without overshoot or oscillation. Furthermore, the coupling effect from the change of the *d*-axis current on the *q*-axis current in the PI system is more dramatic than that in the PDF system.

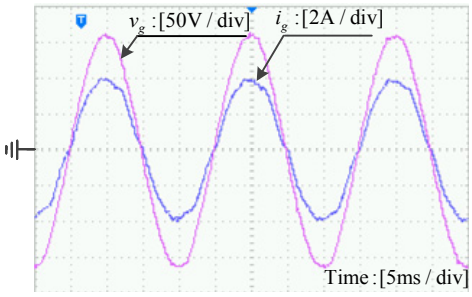

Fig. 24. Steady-state one-phase grid voltage and current of the PDF controlled inverter current feedback system.

When the PI controller is tuned to give a same rise time (1 ms) with the PDF controller, the transient response is shown in Fig. 27. It can be seen that the settling time of the PI system is 8 times that of the PDF system (20 ms versus 2.5 ms). In comparison to the simulation result in Fig. 10, overshoot is damped out by parasitic resistors.

B. PDF for Grid Current Feedback System

Fig. 28 shows the steady-state response of one-phase grid voltage/current of the PDF system when i_{gd} = 4 A. It illustrates that the grid current, with a THD about 3.5%, is synchronized with the grid voltage. The grid voltage adds harmonic components to the grid current but the THD meets the IEEE standard (THD < 5% [1], [3]). In order to mitigate the harmonics, harmonic resonant compensators can be added in the forward path or inner feedback path, but the transient response would be affected [18], [20], [33].

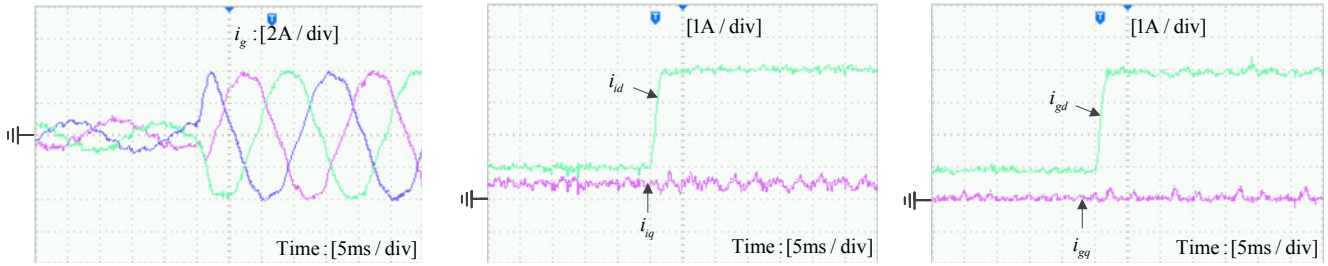

(a) (b) (c)

Fig. 25. Transient response of PDF controlled inverter current feedback system. (a) Grid current. (b) *dq* inverter currents. (c) *dq* grid currents.

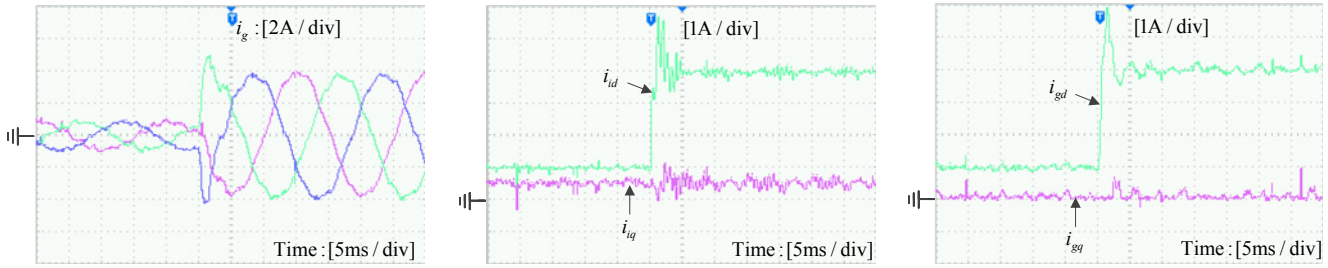

(a) (b) (c)

Fig. 26. Transient response of PI controlled inverter current feedback system. (a) Grid current. (b) *dq* inverter currents. (c) *dq* grid currents.

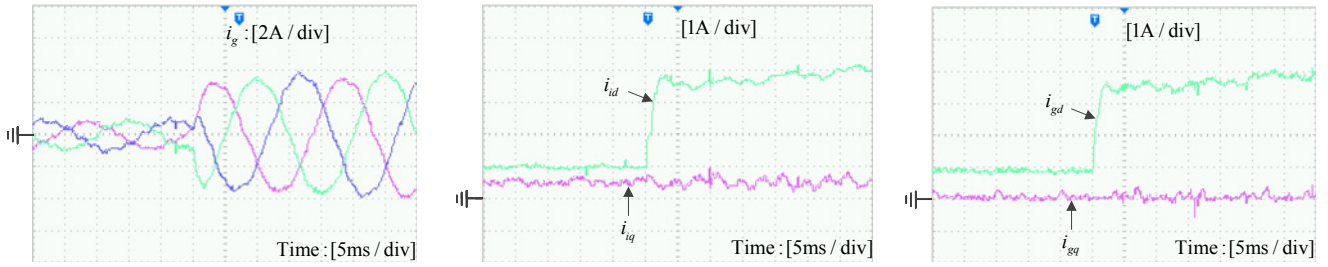

(a) (b) (c)

Fig. 27. Transient response of PI controlled inverter current feedback system with the same rise time as the PDF system. (a) Grid current. (b) *dq* inverter currents. (c) *dq* grid currents.

With f_s = 15000 Hz, the transient response of the PDF system with i_d^* stepping from 1 A to 4 A is shown in Fig. 29. The result indicates a stable operation due to the active damping introduced by the PDF controller. Moreover, there is no overshoot in the transient response. For comparison, the grid current feedback system controlled by PI plus high-pass filter active damping was also examined. For the case with the same parameters as the PDF controller, the transient response of i_{gd} shown in Fig. 30 illustrates a significant overshoot (47%), in a good agreement with the simulation result. For the one with the same rise time (6 ms) as the PDF system, the transient response in Fig. 31 shows a much longer settling time (40 ms versus 12 ms). Moreover, the harmonic disturbance from the grid is much more significant (THD ≈ 10.5% for 1 A and 6.6% for 4 A) due to the lower disturbance rejection ability caused by smaller controller gains. Again, the overshoot is decreased in contrast with the simulation due to parasitic resistors.

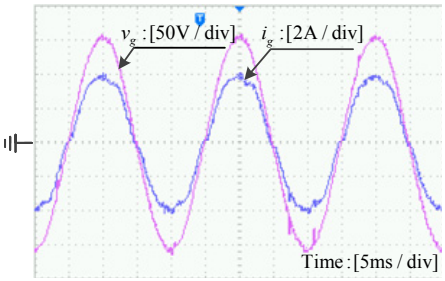

Fig. 28. Steady-state one-phase grid voltage and current of the PDF controlled grid current feedback system.

For the case with f_s = 6000 Hz, the experimental transient responses corresponding to Fig. 22 are shown in Fig. 32. The transient response of the PDF system is smooth without overshoot. The PI controlled systems however exhibit a strong

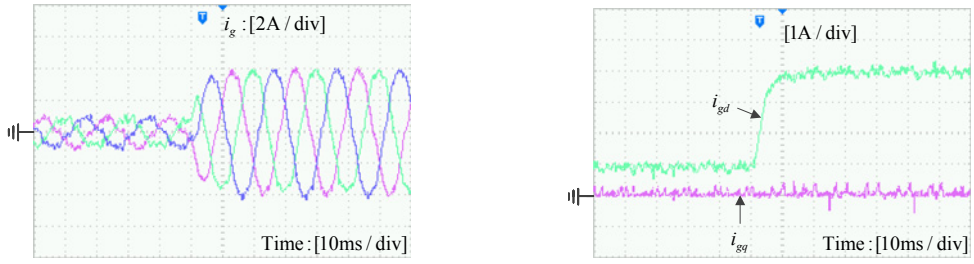

(a) (b)

Fig. 29. Transient response of PDF controlled grid current feedback system (f_s = 15000 Hz). (a) Grid current. (b) *dq* grid currents.

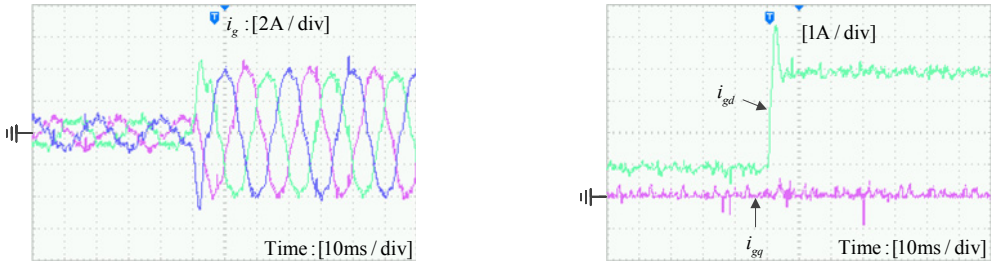

(a) (b)

Fig. 30. Transient response of PI plus high-pass filter active damping controlled grid current feedback system, with the same parameters as the PDF controller (f_s = 15000 Hz). (a) Grid current. (b) *dq* grid currents.

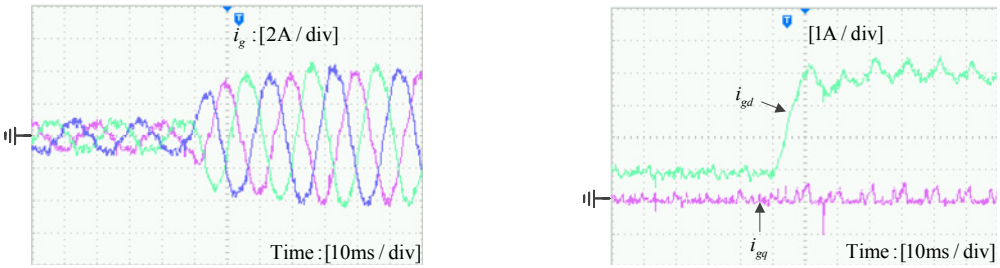

(a) (b)

Fig. 31. Transient response of PI plus high-pass filter active damping controlled grid current feedback system, with the same rise time as the PDF system (f_s = 15000 Hz). (a) Grid current. (b) *dq* grid currents.

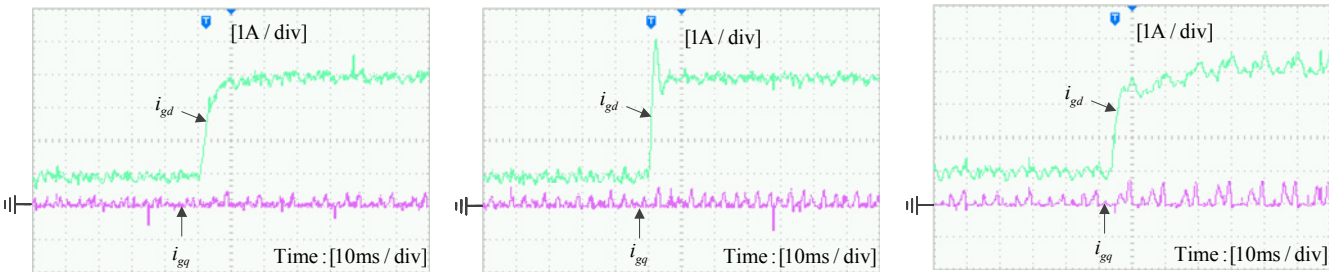

(a) (b) (c)

Fig. 32. Transient responses of grid current feedback systems with f_s = 6000 Hz. (a) PDF. (b) PI plus high-pass filter active damping with the same parameters as the PDF. (c) PI plus high-pass filter active damping with the same rise time as the PDF.

overshoot of 40% or a longer settling time (about 38 ms versus 13 ms of the PDF system) with high harmonic distortions. These results further confirm the advantage of the PDF controller.

VI. Conclusion

The pseudo-derivative-feedback current control has been applied for three-phase grid-connected inverters with *LCL*

filters, as an improved strategy over the PI control in the SRF. Two PDF controllers have been developed for the inverter current feedback system and grid current feedback system, respectively. For the inverter current, a simple PDF controller with identical stability characteristics to that of the PI controller is developed. Compared with the PI controller which can only reduce the transient overshoot by decreasing the controller gains, the PDF controller completely eliminates the overshoot and oscillation over a wide range of controller parameters. For the grid current, a PDF controller with an additional second-order derivative is developed which provides active damping. The stable condition for the controller parameters has been derived by means of the Nyquist stability criterion. A design procedure has been presented that ensures adequate stability margins and satisfactory transient performance. Experimental tests have confirmed the significant performance improvement of the PDF controllers in comparison with the conventional PI control methods.

REFERENCES

[1] F. Blaabjerg, R. Teodorescu, M. Liserre, and A. V. Timbus, "Overview of control and grid synchronization for distributed power generation systems," *IEEE Trans. Ind. Electron.*, vol. 53, no. 5, pp. 1398-1409, Oct. 2006.

[2] T. S. Basso and R. DeBlasio, "IEEE 1547 series of standards: Interconnection issues," *IEEE Trans. Power Electron.,* vol. 19, no. 5, pp. 1159-1162, Sep. 2004.

[3] A. Timbus, M. Liserre, R. Teodorescu, P. Rodriguez, and F. Blaabjerg, "Evaluation of current controllers for distributed power generation systems," *IEEE Trans. Power Electron.*, vol. 24, no. 3, pp. 654-664, Mar. 2009.

[4] J. Dannehl, F. W. Fuchs, and P. B. Thøgersen, "PI state space current control of grid-connected PWM converters with LCL filters," *IEEE Trans. Power Electron.,* vol. 25, no. 9, pp. 2320-2330, Sep. 2010.

[5] J. Wang, J. Yan, L. Jiang, and J. Zou, "Delay-dependent stability of single-loop controlled grid-connected inverters with LCL filters," *IEEE Trans. Power Electron.*, accepted for publication. DOI: 10.1109/TPEL.2015.2401612.

[6] X. Zhang, J. W. Spencer, and J. M. Guerrero, "Small-signal modeling of digitally controlled grid-connected inverters with LCL filters," *IEEE Trans. Ind. Electron.*, vol. 60, no. 9, pp. 3752-3765, Sep. 2013.

[7] M. Liserre, F. Blaabjerg, and S. Hansen, "Design and control of an LCL-filter-based three-phase active rectifier," *IEEE Trans. Ind. Appl.*, vol. 41, no. 5, pp. 1281-1291, Sep./Oct. 2005.

[8] M. Liserre, R. Teodorescu, and F. Blaabjerg, "Stability of photovoltaic and wind turbine grid-connected inverters for a large set of grid impedance values," *IEEE Trans. Power Electron.*, vol. 21, no. 1, pp. 263-272, Jan. 2006.

[9] J. Dannehl, C. Wessels, and F. W. Fuchs, "Limitations of voltage-oriented PI current control of grid-connected PWM rectifiers with LCL filters," *IEEE Trans. Ind. Electron.*, vol. 56, no. 2, pp. 380-388, Feb. 2009.

[10] M. Liserre, A. Dell'Aquila, and F. Blaabjerg, "Genetic algorithm-based design of the active damping for an LCL-filter three-phase active rectifier,"*IEEE Trans. Power Electron.*, vol. 19, no. 1, pp. 76–86, Jan. 2004.

[11] A. Kahrobaeian and Y. Ibrahim, "Robust single-loop direct current control of LCL-filtered converter-based DG units in grid-connected and autonomous microgrid modes," *IEEE Trans. Power Electron.,* vol. 29, no. 10, Oct. 2014.

[12] Wang, X.; Blaabjerg, F.; Loh, P., "Grid-current-feedback active damping for LCL resonance in grid-connected voltage source converters," *IEEE Trans. Power Electron*., accepted for publication. DOI 10.1109/TPEL.2015.2411851

[13] Y. Tang, P. C. Loh, P. Wang, F. H. Choo, F. Gao, and F. Blaabjerg, "Generalized design of high performance shunt active power filter with output LCL filter," *IEEE Trans. Ind. Electron.*, vol. 59, no. 3, pp. 1443-1452, Mar. 2012.

[14] A. G. Yepes, A. Vidal, F. D. Freijedo, J. Malvar, O. Lopez, and J. Doval-Gandoy, "Transient response evaluation of resonant controllers for AC drives," in *Proc. IEEE Energy Convers. Congr. Expo.*, Sep. 2012, pp. 471–478.

[15] J. He and Y. W. Li, "Generalized closed-loop control schemes with embedded virtual impedances for voltage source converters with LC or LCL filters," *IEEE Trans. Power Electron.*, vol. 27, no. 4, pp. 1850-1861, Apr. 2012.

[16] D. N. Zmood and D. G. Holmes, "Stationary frame current regulation of PWM inverters with zero steady-state error," *IEEE Trans. Power Electron.*,vol. 18, no. 3, pp. 814-822, May 2003.

[17] L. Harnefors, A. G. Yepes, A. Vidal, and J. Doval-Gandoy, "Passivity-based stabilization of resonant current controllers with consideration of time delay," *IEEE Trans. Power Electron.*, vol. 29, no. 12, pp. 6260-6263, Dec. 2014.

[18] M. Castilla, J. Miret, A. Camacho, J. Matas, and L. G. de Vicuna, "Reduction of current harmonic distortion in three-phase grid-connected photovoltaic inverters via resonant current control," *IEEE Trans. Ind. Electron.*, vol. 60, no. 4, pp. 1464-1472, Apr. 2013.

[19] X. Wang, F. Blaabjerg, and P. Loh, "Virtual RC damping of LCL-filtered voltage source converters with extended selective harmonic compensation," *IEEE Trans. Power Electron.,* vol. 30, no. 9, pp. 4726-4737, Sep. 2015.

[20] M. Liserre, R. Teodorescu, and F. Blaabjerg, "Multiple harmonics control for three-phase grid converter systems with the use of PI-RES current controller in a rotating frame," *IEEE Trans. Power Electron.*, vol. 21, no. 3, pp. 836–840, May. 2006.

[21] P. Mattavelli, "Synchronous-frame harmonic control for high performance ac power supplies," *IEEE Trans. Ind. Appl.*, vol. 35, no. 3, pp. 864–872, May/Jun. 2001.

[22] C. Lascu, L. Asiminoaei, I. Boldea, and F. Blaabjerg, "Frequency response analysis of current controllers for selective harmonic compensation in active power filters," *IEEE Trans. Ind. Electron.*, vol. 56, no. 2, pp. 337–347, Feb. 2009.

[23] A. G. Yepes, A. Vidal, J. Malvar, O. Lopez, and J. Doval-Gandoy, "Tuning method aimed at optimized settling time and overshoot for synchronous proportional-integral current control in electric machines," *IEEE Trans. Power Electron.*, vol. 29, no. 6, pp. 3041–3054, Jun. 2014.

[24] E. Wu and P. Lehn, "Digital current control of a voltage source converter with active damping of LCL resonance," *IEEE Trans. Power Electron.*, vol. 21, no. 5, pp. 1364–1373, Sep. 2006.

[25] B. Bahrani, M. Vasiladiotis, and A. Rufer, "High-order vector control of grid-connected voltage-source converters with LCL-filters," *IEEE Trans. Ind. Electron.*, vol. 61, no. 6, pp. 2767–2775, Jun. 2014.

[26] X. Bao, F. Zhuo, Y. Tian, and P. Tan, "Simplified feedback linearization control of three-phase photovoltaic inverter with an LCL filter," *IEEE Trans. Power Electron.,* vol. 28, no. 6, pp. 2739-2752, Jun. 2013.

[27] S. A. Khajehoddin and P. K. Jain, "A control design approach for three-phase grid-connected renewable energy resources," *IEEE Trans. Sustain. Energy*, vol. 2, no. 4, pp. 423–432, Oct. 2011.

[28] X. Fu, S. Li, and I. Jaithwa, "Implement optimal vector control for LCL-filter-based grid-connected converters by using recurrent neural networks," *IEEE Trans. Ind. Electron.*, vol. 62, no. 7, pp. 4443-4454, Jul. 2015.

[29] S. Eren, M. Pahlevaninezhad, A. Bakhshai, and P. K. Jain, "Composite nonlinear feedback control and stability analysis of a grid-connected voltage source inverter with LCL filter," *IEEE Trans. Ind. Electron.*, vol. 60, no. 11, pp. 5059-5074, Nov. 2013.

[30] H. Kim, M. Degner, J. Guerrero, F. Briz, and R. Lorenz, "Discrete-time current regulator design for AC machine drives*," IEEE Trans. Ind. Appl.*, vol. 46, no. 4, pp. 1425–1435, Jul./Aug. 2010.

[31] A. Vidal, A.G. Yepes, F. D. Freijedo, O. Lopez, J. Malvar, F. Baneira, and J. Doval-Gandoy, "A method for identification of the equivalent inductance and resistance in the plant model of current-controlled grid-tied converters," *IEEE Trans. Power Electron.*, accepted for publication. DOI 10.1109/TPEL.2015.2395817.

[32] F. Briz, M. W. Degner, and R. D. Lorenz, "Analysis and design of current regulators using complex vectors," *IEEE Trans. Ind. Appl.*, vol. 36, no. 3, pp. 817–825, May/Jun. 2000.

[33] A. Vidal, F. D. Freijedo, A. G. Yepes, P. Fernandez-Comesana, J. Malvar, Ó. Lopez*, et al.*, "Assessment and optimization of the transient response of proportional-resonant current controllers for distributed power generation systems," *IEEE Trans. Ind. Electron*., vol. 60, no. 4, pp. 1367-1383, Apr. 2013.

[34] E. Twining and D. G. Holmes, "Grid current regulation of a three-phase voltage source inverter with an LCL input filter," *IEEE Trans. Power Electron.*, vol. 18, no. 3, pp. 888-895, May 2003.

[35] J. Dannehl, F. W. Fuchs, S. Hansen, and P. B. Thøgersen, "Investigation of active damping approaches for PI-based current control of grid-connected pulse width modulation converters with LCL filters," *IEEE Trans. Ind. Appl*., vol. 46, no. 4, pp. 1509-1517, Jul./Aug. 2010.
[36] D. Pan, X. Ruan, C. Bao, W. Li, and X. Wang, "Capacitor-current-feedback active damping with reduced computation delay for improving robustness of LCL-type grid-connected inverter," *IEEE Trans. Power Electron.*, vol. 29, no. 7, pp. 3414-3427, Jul. 2014.
[37] L. Harnefors, A. G. Yepes, A. Vidal, and J. Doval-Gandoy, "Passivity based controller design of grid-connected VSCs for prevention of electrical resonance instability," *IEEE Trans. Ind. Electron.*, vol. 62, no. 2, pp. 702–710, Feb. 2015.
[38] R. Peña Alzola, M. Liserre, F. Blaabjerg, R. Sebastian, J. Dannehl, and F. W. Fuchs, "Systematic design of the lead-lag network method for active damping in LCL-filter based three phase converters," *IEEE Trans. Ind. Inf*., vol. 10, no. 1, pp. 43–52, Feb. 2014.
[39] C. Bao, X. Ruan, X. Wang, W. Li, D. Pan, and K. Weng, "Step-by-step controller design for LCL-Type Grid-Connected inverter with capacitor-current-feedback active-damping," *IEEE Trans. Power Electron.,* vol. 29, no. 3, pp. 1239-1253, Mar. 2014.
[40] F. Liu, Y. Zhou, S. Duan, J. Yin, B. Liu, and F. Liu, "Parameter design of a two-current-loop controller used in a grid-connected inverter system with LCL filter," *IEEE Trans. Ind. Electron.*, vol. 56, no. 11, pp. 4483-4491, Nov. 2009.
[41] J. Xu, S. Xie, and T. Tang, "Active damping-based control for grid-connected LCL-filtered inverter with injected grid current feedback Only," *IEEE Trans. Ind. Electron.*, vol. 61, no. 9, pp. 4746-4758, Sep. 2014.
[42] M. Hanif, V. Khadkikar, W. Xiao, and J. L. Kirtley, "Two degrees of freedom active damping technique for LCL filter-based grid connected PV systems," *IEEE Trans. Ind. Electron.*, vol. 61, pp. 2795-2803, Jun. 2014.
[43] J.-S. Yim, S.-K. Sul, B.-H. Bae, N. Patel, and S. Hiti, "Modified current control schemes for high-performance permanent-magnet AC drives with low sampling to operating frequency ratio," *IEEE Trans. Ind. Appl.*, vol. 45, no. 2, pp. 763–771, Mar./Apr. 2009.
[44] B.-H. Bae and S.-K. Sul, "A compensation method for time delay of full digital synchronous frame current regulator of PWM AC drives," *IEEE Trans. Ind. Appl.*, vol. 39, no. 3, pp. 802–810, May/Jun. 2003.
[45] S. G. Parker, B. P. McGrath, and D. G. Holmes, "Regions of active damping control for LCL filters," *IEEE Trans. Ind. Appl.*, vol. 50, pp. 424-432, Jan/Feb. 2014.
[46] R. M. Phelan, *Automatic control systems*: Cornell University, 1977.
[47] W. Phipps, R. Duke, and M. J. Harrison, "A proposal for a new generation power converter with pseudo-derivative control," in *Proc. Int. Telecom. Energ. Conf,* 2006, pp. 1-5.
[48] D. Y. Ohm, "Analysis of PID and PDF compensators for motion control systems," in *Conf. Rec. IEEE-IAS Annu. Meeting*, Vol. 3, pp. 1923-1929, Oct. 1994.
[49] J. Wang and J. Yan, "Using virtual impedance to analyze the stability of LCL-filtered grid-connected inverters", in *Proc. IEEE ICIT*, Seville, Spain, Mar. 17-19, 2015, pp. 1220-1225.
[50] Y. Tang, P. C. Loh, P. Wang, F. H. Choo, and F. Gao, "Exploring inherent damping characteristic of LCL-filters for three-phase grid-connected voltage source inverters," *IEEE Trans. Power Electron.*, vol. 27, no. 3, pp. 1433-1443, Mar. 2012.
[51] X. Wang, X. Ruan, S. Liu, and C. K. Tse, "Full feedforward of grid voltage for grid-connected inverter with LCL filter to suppress current distortion due to grid voltage harmonics," *IEEE Trans. Power Electron.*, vol. 25, no. 12, pp. 3119–3127, Dec. 2010.
[52] N. He, J. Zhang, Y. Zhu, G. Shen, and D. Xu, "Weighted average current control in three-phase grid inverter with LCL filter," *IEEE Trans. Power Electron.*, vol. 28, no. 6, pp. 2785-2797, Jun. 2013.
[53] D. G. Holmes, T. A. Lipo, B. P. McGrath, and W. Y. Kong, "Optimized design of stationary frame three phase AC Current regulators," *IEEE Trans. Power Electron.*, vol. 24, no. 11, pp. 2417-2426, Nov. 2009.

Jianguo Wang (S'14) was born in Jiangxi Province, China, in 1988. He received the B.S. and M.S. degrees in electrical engineering from Dalian University of Technology, Dalian, China, in 2010 and 2013, respectively.

Since 2012, he has been with the Department of Electrical Engineering and Electronics, University of Liverpool, UK. His research interests include the control of power electronics and renewable energy generation system.

Jiu Dun Yan (M'03) received the BEng and MEng degrees from the Department of Engineering Mechanics, Tsinghua University, Beijing, China, in 1986 and 1988, respectively. He then worked in Xi'an High Voltage Research Institute (now XIHARI) in China for 6 years, engaged in the R&D of high voltage switchgear, before he joined the University of Liverpool where he studied for and was awarded in 1998 his PhD degree.

He is currently a Reader at the University of Liverpool with research interests in switching arcs and its numerical modelling, thermal management for high voltage equipment, intelligent circuit breakers, electric discharges under HVDC stress and power electronics based inverter systems for grid connection of renewable power generation systems. He has published a total of 115 refereed journal and conference papers.

Lin Jiang (M'00) received the B.Sc. and M.Sc. degrees from Huazhong University of Science and Technology, Wuhan, China, in 1992 and 1996, respectively, and the Ph.D. degree from The University of Liverpool, Liverpool, U.K., in 2001, all in electrical engineering.

He was a Postdoctoral Research Assistant with The University of Liverpool, Liverpool, U.K., from 2001 to 2003 and a Postdoctoral Research Associate with the Department of Automatic Control and Systems Engineering, University of Sheffield, Sheffield, U.K., from 2003 to 2005. He was a Senior Lecturer with the University of Glamorgan from 2005 to 2007 and joined the University of Liverpool in 2007. Currently, he is a Senior Lecturer with The University of Liverpool. His current research interests include control and analysis of power system, smart grid, and renewable energy.